J Electroceram (2007) 19:187–194
DOI 10.1007/s10832-007-9187-2

Effect of Bi_2O_3 and Sb_2O_3 on the grain size distribution of ZnO

Yeh-Wu Lao · Shu-Ting Kuo · Wei-Hsing Tuan

Received: 7 November 2006 / Accepted: 25 June 2007 / Published online: 1 August 2007

Abstract In the present study, the effect of Bi_2O_3 and Bi_2O_3+Sb_2O_3 additions on the size distribution of ZnO grains is investigated. Without the usage of a powder bed, the addition of Bi_2O_3 provides a transient liquid phase that enhances the densification. The residual Bi segregates alters the surface/grain boundary energy ratio, which encourages the ZnO grains to grow. The size variation is also increased. The addition of both Bi_2O_3 and Sb_2O_3 induces the formation of pyrochlore, spinel and inversion boundary. Their presence reduces not only the average grain size, but also the size variation.

Keywords Zinc oxide · Grain growth · Varistor

1 Introduction

Zinc oxide (ZnO) based varistors with multilayer structure are now frequently used as the surge-protection devices in many 3C (communication, computer, consumer) electronic products [1–4]. To fulfill the requirement on miniaturization, the operating voltage of such multilayered varistor (MLV) is also low. Sometimes it may be even as low as 5.5 V. Since the breakdown voltage (or more precisely the transition voltage [1]) of one single insulating grain boundary in varistor is around 3.5 V [1–3], only a few grains are allowed to squeeze into the inner electrodes. Contrary to other multilayered ceramic devices, the ZnO grains within MLV are allowed to grow. By having larger ZnO grains, the thickness of each ceramic layer can be thicker. There is thus no need to prepare very thin ceramic layer for the MLV devices. However, once the grains start to grow, a size variation is bound to form. The electrical current tends to pass through the part with least number of grain boundaries, as demonstrated in Fig. 1. To narrow down the size scattering, especially to reduce the number of large grains, is the key to ensure the reliability of MLV.

The grain size distribution in a sintered body depends strongly on the particle size distribution of starting powder, the uniformity of sintering additive and of second phase particles [4, 5]. The size of grains usually shows a normal distribution, as shown in Fig. 2. The extent of scattering in grain size can be characterized by using the value of standard deviation. Since the amount of large grains plays the most important role on the breakdown behavior of ZnO-based varistor (see Fig. 1), two parameters are introduced in the present study to estimate the amount of large grains. These two parameters are $D+\sigma$ and $D+2\sigma$ (D is average grain size, σ the standard deviation, see Fig. 2). Since the area fraction, rather than the number fraction, of large grains dominates the breakdown behavior of ZnO varistor; the area fraction is used in the present study to characterize the microstructure uniformity.

Since Bi_2O_3 and Sb_2O_3 are frequently used as the sintering additives for ZnO based varistors [1, 2, 6, 7], their effects on the sintering behavior, grain boundary chemistry and electrical performance of ZnO have attracted much attention [1, 2, 8]. However, the effect of Bi_2O_3 and Sb_2O_3 on the grain size distribution has received relatively less attention. In the present study, the effect of Bi_2O_3 and Sb_2O_3 on the size distribution of ZnO grains after sintering is investigated.

Y.-W. Lao · S.-T. Kuo · W.-H. Tuan (✉)
Department of Materials Science and Engineering,
National Taiwan University,
Taipei, Taiwan
e-mail: tuan@ccms.ntu.edu.tw

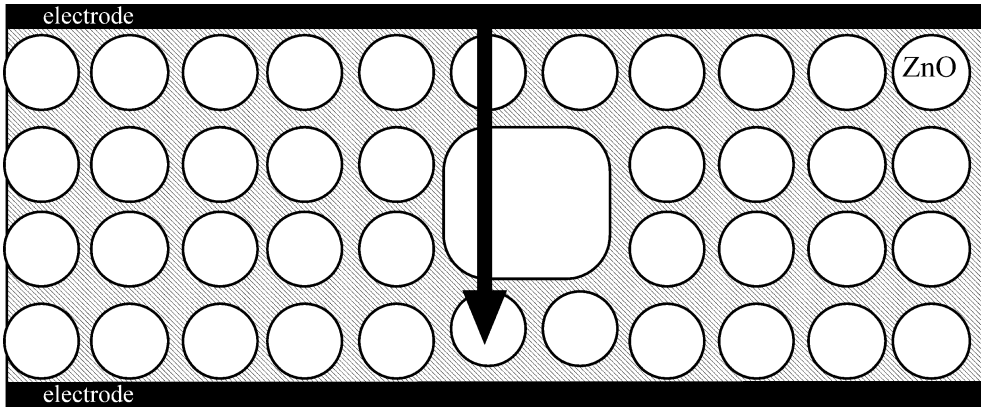

Fig. 1 Schematic to show that the electrical current tends to pass through the area with less grain boundaries

2 Experimental procedure

A high-purity ZnO powder was mixed with various amounts of Bi_2O_3 or both Bi_2O_3 and Sb_2O_3 by ball milling in ethyl alcohol for 4 hours. The starting amount of Bi_2O_3 in the ZnO–Bi_2O_3 specimens was 0.36 and 0.72 mol%. For the ZnO–Bi_2O_3–Sb_2O_3 specimens, the amount of Bi_2O_3 was 0.36, 0.72 and 2 mol%. The amount of Sb_2O_3 was doubled that of Bi_2O_3. After drying, the dried lumps passed a #150 sieve to remove the agglomerates. The green compacts, with the diameter of 10 mm and thickness of 3 mm, were formed by uniaxial pressing at 50 MPa. Sintering was performed within a box furnace from 800 to 1300°C for 1 h. No powder bed was used. The effect of powder bed will be addressed in a separate paper. The heating and cooling rates were 5°C/min. The density was determined with the water displacement method. The cross-section of the specimens were ground with silicon carbide particles and polished with alumina particles. The grain boundaries were revealed by soaking the polished section in dilute hydrochloric acid for several seconds. The microstructure was observed by using scanning electron microscopy (SEM). The SEM micrographs were then digitized by using a scanner. The image analysis was performed on the digitized images in order to determine the area of each grain. Over 500 grains were measured for each composition. The equivalent circular diameter was determined from the area, assuming that each grain was spherical. The 3-dimensional mean grain size was calculated by multiplying the mean equivalent circular diameter by 1.5. The chemical composition of the specimens was estimated by using the energy dispersive spectroscopy (EDX) and electron probe microanalysis (EPMA).

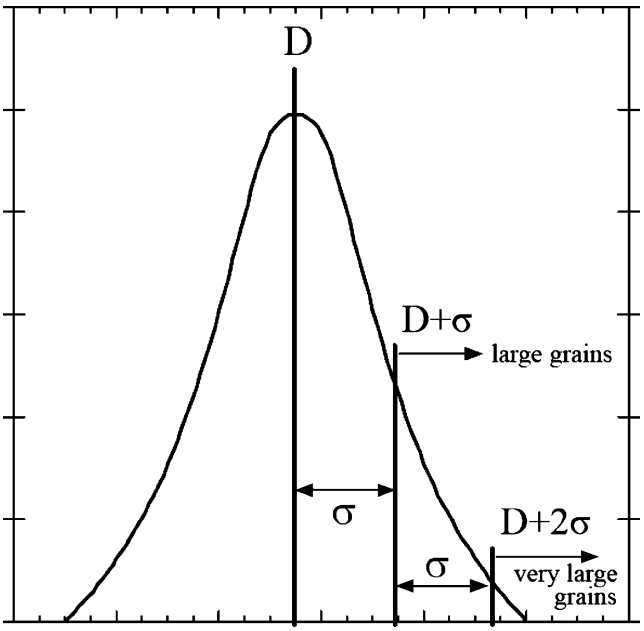

Fig. 2 Schematic of a normal grain size distribution, where D is the average grain size and σ the standard deviation. The definitions for the large grains ($>D+\sigma$) and very large grains ($>D+2\sigma$) are also shown

3 Results

Figure 3 shows the weight loss of the ZnO–Bi_2O_3 and ZnO–Bi_2O_3–Sb_2O_3 specimens after firing at elevated temperatures for 1 h. The Bi_2O_3 in the ZnO–Bi_2O_3 specimens starts to vaporize from a temperature as low as 800°C. The weight loss of the ZnO–Bi_2O_3–Sb_2O_3 specimens increases rapidly from 1000°C; the co-doping of Sb_2O_3 increases the vaporization resistance of the specimens.

Figure 4 shows the XRD patterns of the ZnO–Bi_2O_3 specimens after firing at various temperatures. There is no Bi_2O_3 found as the ZnO–Bi_2O_3 specimens are heated above 900°C. Figure 5 shows the XRD patterns of the ZnO–Bi_2O_3–Sb_2O_3 specimens. There is no Bi_2O_3 found either, as the firing temperature is higher than 700°C. A pyrochlore phase, $Zn_2Bi_3Sb_3O_{14}$, is found instead. The β-phase of spinel, $Zn_7Sb_2O_{12}$, is started to form above 900°C. As the firing temperature is higher than 1000°C, the increase of spinel intensity is accompanied by the

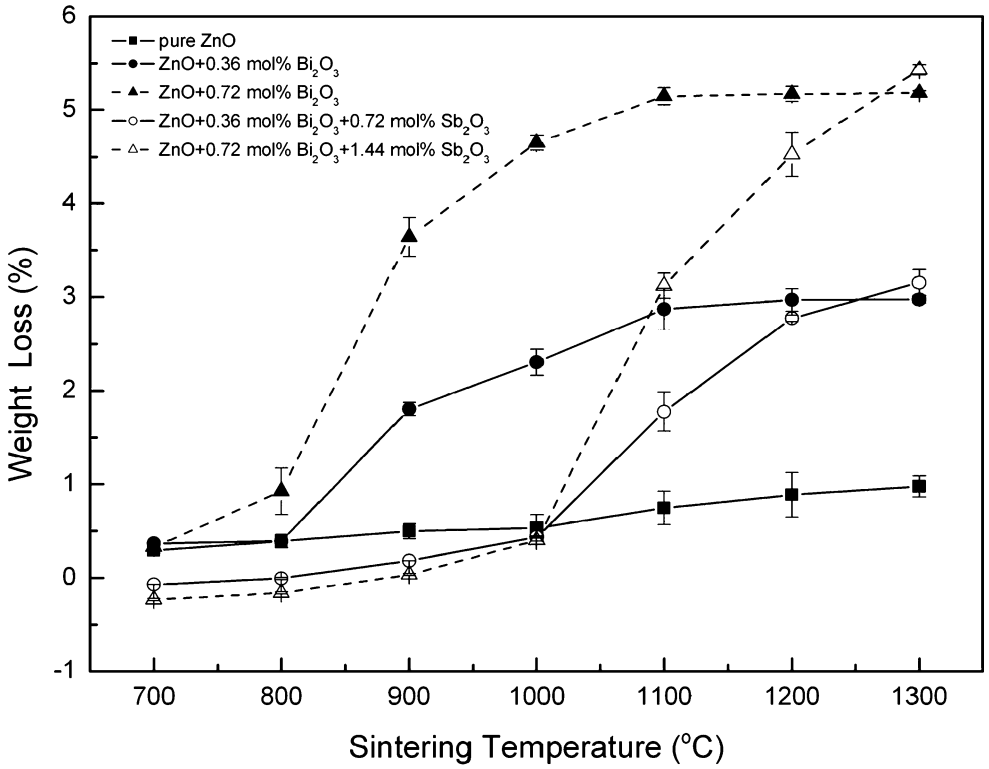

Fig. 3 Weight loss of ZnO, $ZnO–Bi_2O_3$ and $ZnO–Bi_2O_3–Sb_2O_3$ specimens after firing at the indicated temperatures for 1 h

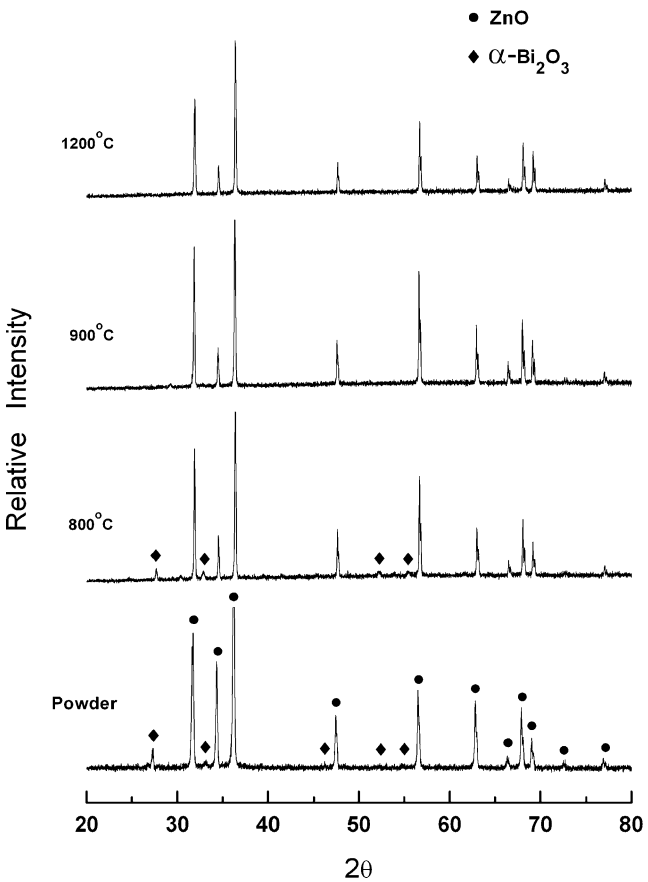

Fig. 4 XRD patterns of ZnO–0.72 mol% Bi_2O_3 specimens after sintering at the indicated temperatures for 1 h

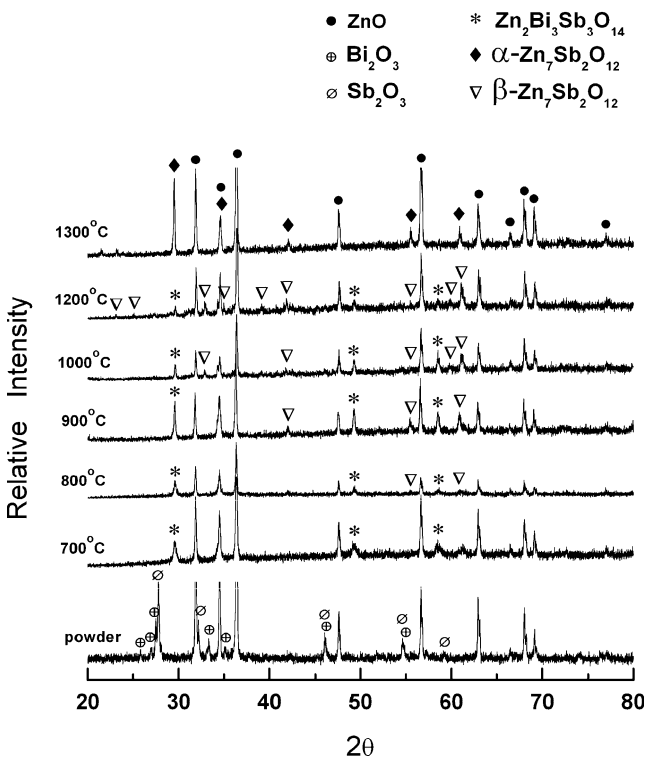

Fig. 5 XRD patterns of ZnO–2 mol% Bi_2O_3–4 mol% Sb_2O_3 specimens after sintering at the indicated temperatures for 1 h

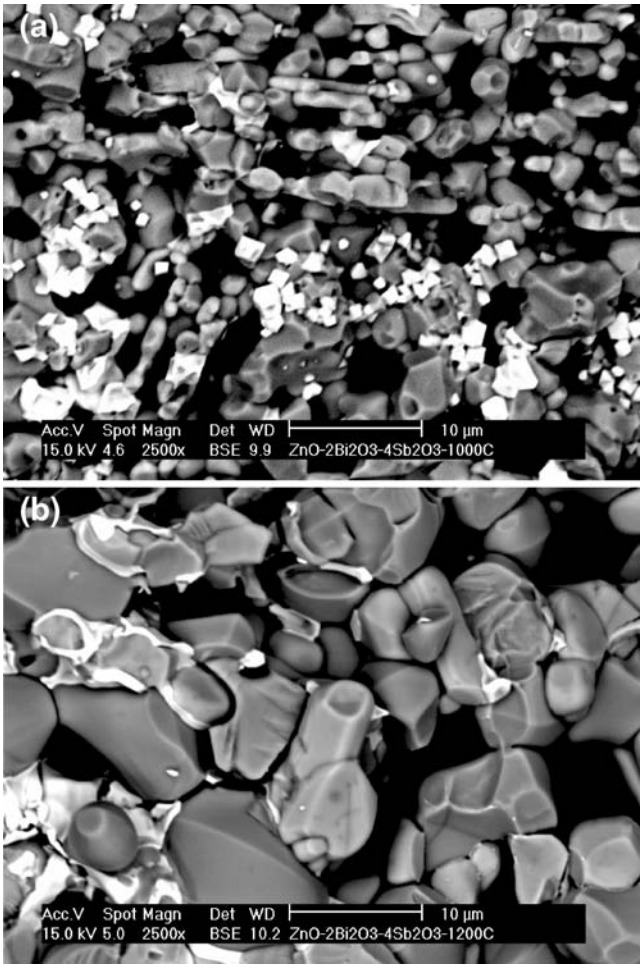

Fig. 6 Fracture surfaces of ZnO–2 mol% Bi_2O_3–4 mol% Sb_2O_3 specimens after sintering at (**a**) 1000°C and (**b**) 1200°C for 1 h

consumption of the pyrochlore. As the specimen is heated above 1200°C, only α-type spinel can be found.

The crystalline structure of pyrochlore is cubic [9]; the pyrochlore particle is cubic in shape at the beginning of its formation. Though the starting pyrochlore particles are relatively small (see Fig. 6(a)); the coarsening of the second phase particles (pyrochlore and spinel) is very rapid as the sintering temperature is higher than 1100°C (see Fig. 6(b)). Furthermore, these second phase particles tend to form large clusters. Figure 7 shows the apparent density of the specimens after sintering at various temperatures. The addition of Bi_2O_3 enhances the densification of ZnO. However, the co-doping of Bi_2O_3 and Sb_2O_3 exhibits reverse trend.

Figure 8 shows the typical micrographs of the ZnO, ZnO–Bi_2O_3 and ZnO–Bi_2O_3–Sb_2O_3 specimens after sintering at 1300°C for 1 h. The back-scattered mode of the SEM technique reveals no second phase at the grain boundaries in the ZnO–Bi_2O_3 specimen. The EDX that incorporated with the SEM reveals no trace of Bi_2O_3 either. However, a small amount of Bi_2O_3, around several hundred ppm, can be found at the grain boundaries by applying the EPMA analysis. It indicates that a small amount of Bi_2O_3 remains at the grain boundaries after sintering.

For the ZnO–Bi_2O_3–Sb_2O_3 specimens, apart from the spinel phase, as confirmed by the EDX analysis, many inversion boundaries (IB) can be observed within the ZnO grains (see Fig. 8(c)). The presence of IB is the characteristic microstructure for the Sb_2O_3-doped ZnO [10, 11]. Furthermore, its presence is revealed only by

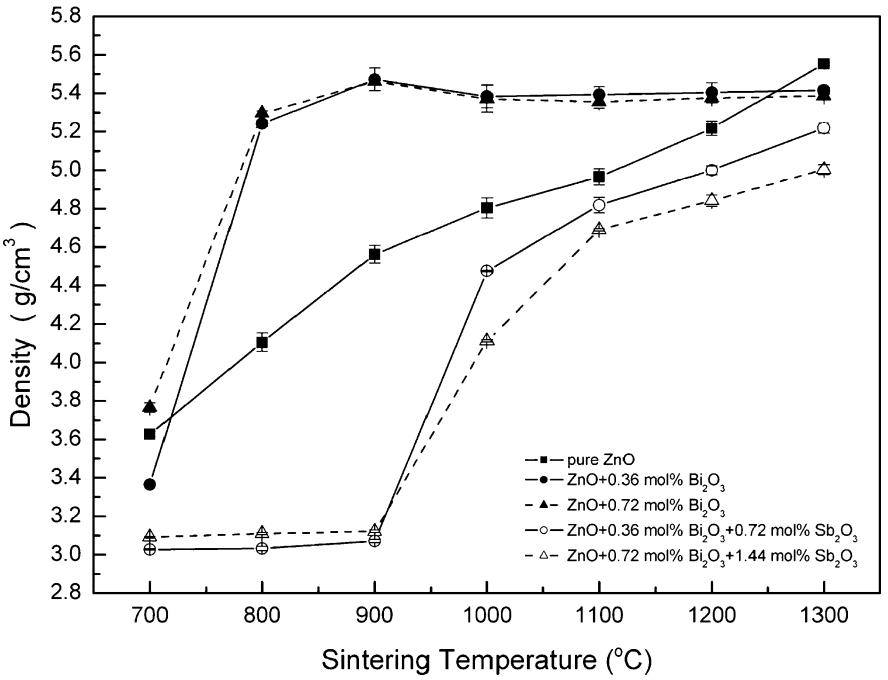

Fig. 7 Absolute density of ZnO, ZnO–Bi_2O_3 and ZnO–Bi_2O_3–Sb_2O_3 specimens after sintering at the indicated temperatures for 1 h

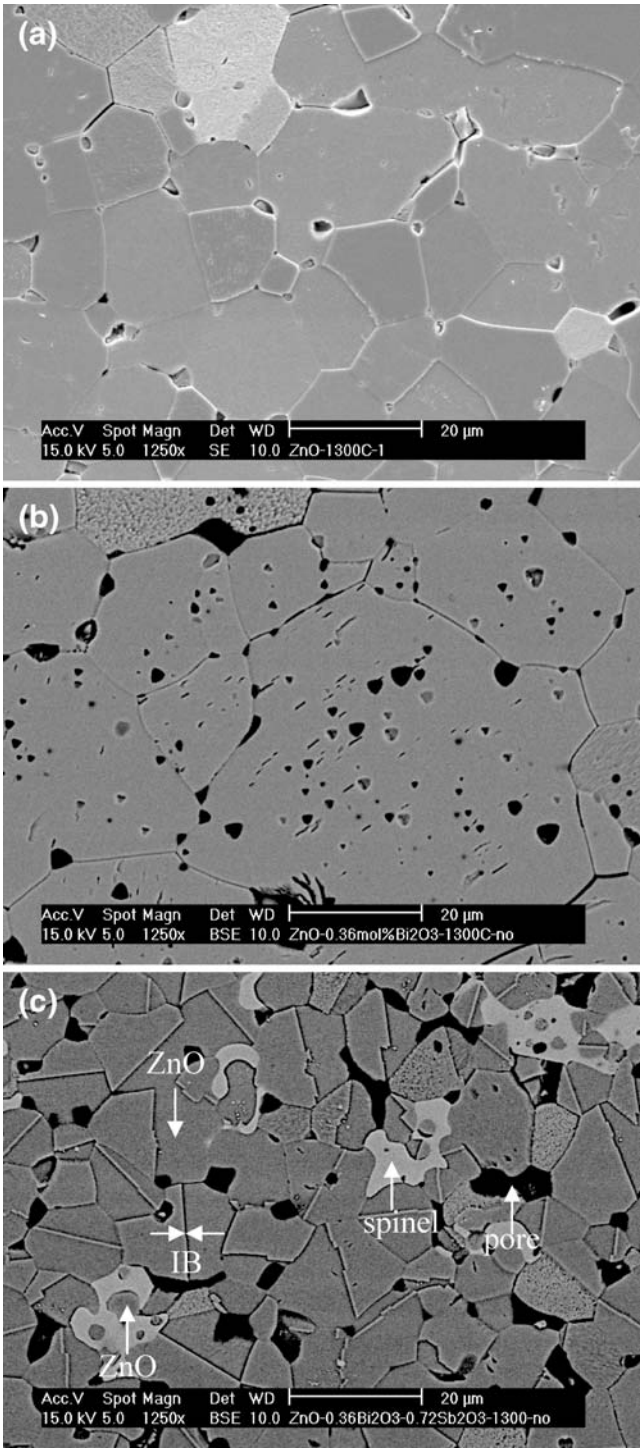

Fig. 8 Typical micrographs of (**a**) ZnO, (**b**) ZnO–0.36 mol% Bi_2O_3 and (**c**) ZnO–0.36 mol% Bi_2O_3–0.72 mol% Sb_2O_3 specimens after sintering at 1300°C for 1 h

etching with dilute HCl solution [11]. Figure 9 shows the corresponding curves for the size distribution of ZnO grains in the specimens shown in Fig. 8. The microstructure characteristics of the specimens are shown in Table 1.

Figure 10 shows the I–V curves for the ZnO–Bi_2O_3 and ZnO–Bi_2O_3–Sb_2O_3 specimens. The I–V curves demonstrate typical nonlinear characteristics for ZnO-based varistor, though their nonlinearity exponent α values are rather low, around 3.

4 Discussion

The melting point of Bi_2O_3 and Sb_2O_3 is 825 and 570°C, respectively [12]. The eutectic temperature of ZnO–Bi_2O_3 is only 740°C [13]; a liquid is thus formed below 800°C in the ZnO–Bi_2O_3 specimens. As soon as the eutectic liquid is formed, the weight loss starts to pick up. It indicates that the vaporization of Bi_2O_3 is started immediately after the eutectic liquid is formed. The formation of the eutectic liquid enhances the densification of the ZnO, though the presence of such large amount of liquid is momentary.

The oxidation of Sb_2O_3 at low temperatures [2], <900°C, induces a small weight gain (see Fig. 3). For the ZnO–Bi_2O_3–Sb_2O_3 specimens, as soon as Sb_2O_3 is melted, solid pyrochlore particles are formed. Though the cubic pyrochlore ($Zn_2Bi_3Sb_3O_{14}$) particles are small in the beginning (see Fig. 6(a)), their formation consumes the Bi_2O_3. Since the formation of solid pyrochlore is taken place below 800°C; the weight loss of the ZnO–Bi_2O_3–Sb_2O_3 specimens is thus slowed down. As the temperature is higher than 1000°C, the spinel phase, $Zn_7Sb_2O_{12}$, is formed. The formation of spinel is accompanied with the formation of Bi_2O_3 liquid as the reaction shown below [14]

$$17\ ZnO + 2\ Zn_2Bi_3Sb_3O_{14} \rightarrow 3\ Zn_7Sb_2O_{12} + 3\ Bi_2O_3 \quad (1)$$

The generation of the Bi_2O_3-rich liquid induces the formation of capillary forces, which brings the second phase together to form cluster (see Fig. 6(b)). Such clusters tend to survive till the end of sintering (see Fig. 8(c)), though the decrease of pyrochlore and the increase of spinel are taken place simultaneously. The size of the second phase clusters is large; and the distribution of the second phase is not uniform (see Fig. 8(c)). As soon as the Bi_2O_3-rich liquid is formed, the vaporization is started. The weight loss of the ZnO–Bi_2O_3–Sb_2O_3 specimens thus jumps as the temperature is raised above 1000°C (see Fig. 3), confirming that the reaction 1 is taken place from a temperature around 1000°C. The formation of the Bi_2O_3-rich liquid enhances the densification of the specimens. It indicates that the Bi_2O_3-rich liquid is an effective liquid to enhance the densification of ZnO specimens; though its presence is temporary. However, the co-doping of Bi_2O_3 and Sb_2O_3 diminishes the densification of ZnO (see Fig. 7). The addition of both Bi_2O_3 and Sb_2O_3 induces the formation of

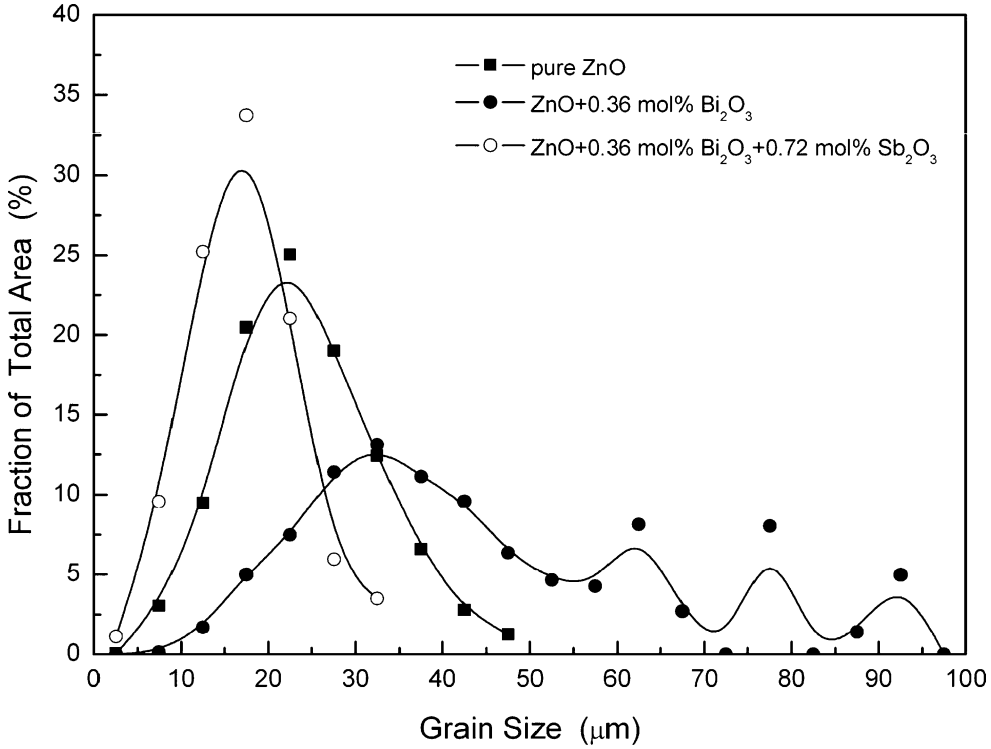

Fig. 9 Size variation (in area fraction) of ZnO grains in the specimens shown in Fig. 8

two second phases such as pyrochlore and spinel during the heating-up stage. The presence of the second phases increases the diffusion distance between ZnO grains. The densification of ZnO is thus retarded due to the presence of the second phases.

Table 1 shows the microstructural characteristics of the ZnO, ZnO–Bi_2O_3 and ZnO–Bi_2O_3–Sb_2O_3 specimens after sintering. Though the coefficient of variation (C.V.) and the amount of large grains ($>D+\sigma$) of the three systems are very close to each other, the amount of very large grains ($>D+2\sigma$) reveals distinct difference. The addition of Bi_2O_3 into ZnO increases significantly the amount of very large grains. The breakdown is taken place at the area with the least grain boundaries; the amount of very large grains is thus critical especially when the layer thickness is small. It demonstrates that the $D+2\sigma$ parameter is a valuable index to quantify the extent of microstructure uniformity.

It is also worth noting that the change of pore shape as Bi_2O_3 is added into ZnO. The shape of the pores is governed by the magnitude of the dihedral angle (Ψ), which is controlled by the balance between the surface energy (γ_s) and grain boundary energy (γ_{gb}), as demonstrated in Fig. 11 and the following equation [15]

$$\gamma_{gb} = 2\gamma_s \cos\frac{\Psi}{2} \tag{2}$$

The addition of Bi_2O_3 may change both the values of surface energy and grain boundary energy to different extent. The dihedral angle is therefore altered after the

Table 1 Average grain size $(\overline{G})$, coefficient of size variation (C.V.), area fraction of coarse grain ($>D+\sigma$, $>D+2\sigma$), breakdown voltage of specimen (E_b) and of one grain boundary (V_{gb}) of the ZnO, ZnO–0.36mol% Bi_2O_3 and ZnO–0.36mol%Bi_2O_3–0.72%Sb_2O_3 specimens sintered at 1300°C for 1 h.

Compositions	Average grain size $(\overline{G})$/μm	C.V/ %	Large grains $(>\overline{G}+\sigma)$/%	Very large grains $(>\overline{G}+2\sigma)$/%	E_b	V_{gb}	V_{gb1}[a]	V_{gb2}[b]
Pure ZnO	18	45	41	14	–	–	–	–
ZnO—0.36 mol% Bi_2O_3	29	51	44	26	97	0.28	0.42	0.57
ZnO–0.36 mol% Bi_2O_3–0.72 mol% Sb_2O_3	12	50	44	14	427	0.5	0.76	1.01

[a] The definition of V_{gb1} can be found in Eq. 4.
[b] The definition of V_{gb2} can be found in Eq. 5.
σ Standard deviation, C.V. = (σ/D) %

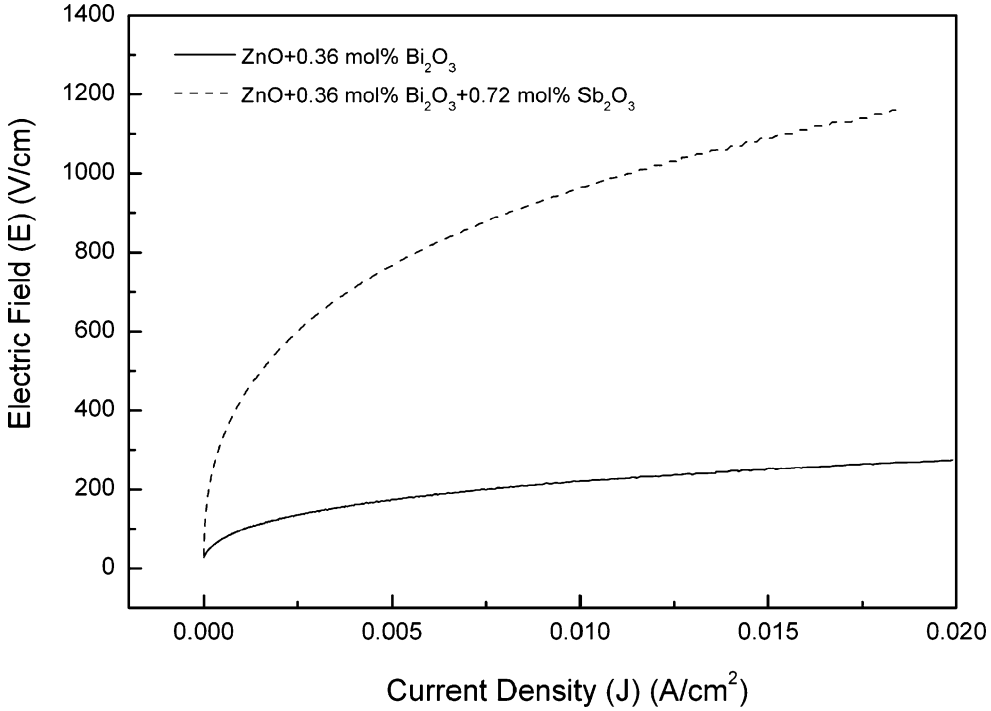

Fig. 10 *J–E* curves of ZnO–0.36 mol% Bi_2O_3 and ZnO–0.36 mol% Bi_2O_3–0.72 mol% Sb_2O_3 specimens prepared by sintering at 1300°C for 1 h

addition of Bi_2O_3. A small amount of Bi_2O_3, around 300 ppm, is detected by the EPMA technique at the boundaries of ZnO grains, suggesting the presence of Bi_2O_3 liquid phase or Bi segregates at the boundaries. Previous report indicated that the Bi_2O_3-rich liquid could form a very thin (around 1~1.5 nm) film at the boundaries of ZnO grains [13]. Though the Bi_2O_3-rich phase is amorphous, the film is an equilibrium one for its low energy. Therefore, the addition of Bi_2O_3 reduces γ_{gb}, which consequently increases the value of dihedral angle (See Fig. 11(b)). The pores in the Bi_2O_3-doped ZnO specimens are therefore more rounded in shape.

As the dihedral angle is increased, the ability of the pore to pin the grain boundary is reduced [15]. Therefore, many pores are trapped within ZnO grains, indicating that the grains boundaries sweep easily through the ZnO grains and left behind many pores. Since the pores are no longer able to attach to the grain boundaries, the size of ZnO grains in the ZnO–Bi_2O_3 specimens is larger than that in the ZnO specimen. However, the size variation of the ZnO grains is also increased due to the change of dihedral angle (see Fig. 9 and Table 1). Bismuth oxide tends to vaporize at elevated temperature; the residual Bi_2O_3 amount is low after sintering at 1300°C. Previous study suggested that such thin Bi_2O_3 layer locates at the most boundaries [13]. The scattering of the ZnO grain size may thus relate to the size variation of pores.

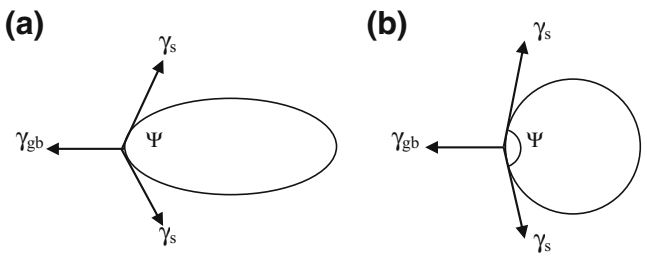

Fig. 11 Schematics of the pore in the sintered (**a**) ZnO and (**b**) ZnO–Bi_2O_3 specimens

The presence of second phases, though their distribution is not uniform at all (see Figs. 6(b) and 8(c)), can prohibit the growth of ZnO grains [7, 16–19]. It is also worth noting that IB is found in almost every ZnO grains. The presence of inversion boundary can also prohibit the growth of ZnO grains [10, 11, 16–18]. Since the IB can be found in most ZnO grains and the distribution of second phase is not uniform, suggesting that the presence of IB is the key parameter to prohibit the growth of ZnO grains. Its presence also reduces the size variation of the ZnO grains. Since the growth of each ZnO grain is prohibited by the presence its IB, the distribution of the ZnO grains in the ZnO–Bi_2O_3–Sb_2O_3 specimens is thus very close to that of the ZnO specimen (see Table 1).

The higher breakdown electric field, E_b, for the ZnO–Bi_2O_3–Sb_2O_3 specimen is contributed by its smaller grain size, see Table 1. The breakdown voltage of each grain boundary V_{gb}, is usually calculated by using the following equation as [20]

$$V_{gb} = \frac{E_b}{(t/\overline{G})} \tag{3}$$

where t is the thickness of specimen and $(\overline{G})$ the average grain size. By using the above the equation, the size variation is ignored. As the thickness of the specimen is large, such assumption may be acceptable. However, as the thickness of the each ZnO-based layer is small, as the case for multilayer varistor, such assumption may result in serious underestimation. Sung et al. [4] had proposed to use the following equation to calculate the breakdown voltage for each grain boundary as

$$V_{gb1} = \frac{E_b}{t/(\overline{G}+\sigma)} \tag{4}$$

where σ is one standard deviation of the grain size. In the present study, we propose to use the following equation to estimate the breakdown voltage for each grain boundary as

$$V_{gb2} = \frac{E_b}{t/(\overline{G}+2\sigma)} \tag{5}$$

The calculated values are shown in Table 1. By considering the fact that the electrical breakdown is dominated by a few large grains; the breakdown voltage calculated by using Eq. 5 is higher than those using Eqs. 3 and 4. Though the exact value for V_{gb} awaits further evidence on the direct measurement of each grain boundary, the above calculations demonstrate that the importance of the size variation on the estimation of breakdown voltage for each grain boundary.

The addition of Sb_2O_3 increases the breakdown electric field (E_b) and breakdown voltage of grain boundary (V_{gb}) significantly (see Table 1). The addition of Sb_2O_3 reduces the size of ZnO grains as well as their scatters. The number of very large grains is smaller in the ZnO–Bi_2O_3–Sb_2O_3 system. The Eq. 4, instead of Eq. 5, may be used to calculate the breakdown voltage of each grain boundary for the ZnO–Bi_2O_3–Sb_2O_3 specimen. It is of interest to note as the Eq. 4 is used to calculate the grain boundary for each grain boundary of the ZnO–Bi_2O_3–Sb_2O_3 specimen, the resulted value is close to the value calculated by using Eq. 5 for the ZnO–Bi_2O_3 specimen. It again demonstrates that the size variation plays an important role on the electrical properties of the ZnO-based material.

5 Conclusions

The effect of Bi_2O_3 and Sb_2O_3 addition on the microstructure uniformity of ZnO is investigated in the present study. The amount of very large grains, the grain larger than the average grain size plus two times that of standard deviation ($>D+2\sigma$), is proposed as an index to quantify the microstructure uniformity. The addition of Bi_2O_3 reduces the grain boundary energy that results in an increase of dihedral angle; the pores are no longer able to prohibit the grain growth. The scatter of the pore size induces larger grain size variation. The addition of Sb_2O_3 induces the formation of inversion boundary in every ZnO grains, which effectively reduces the average grain size and the scatter of grain size.

Acknowledgments The present study was supported by the National Science Council, Taiwan through the contract number of NSC94-2216-E-002-014. The technical help from Huey-Ru Chen, Walsin Technology Corporation, Kaohsiung, Taiwan, is highly appreciated.

References

1. D.R. Clarke, J. Am. Ceram. Soc. **82**, 485 (1999)
2. J. Ott, A. Lorenz, M. Harrer, E.A. Preissner, C. Hesse, A. Feltz, A. H. Whitehead, M. Schreiber, J. Electroceram. **6**, 135 (2001)
3. E. Olsson, G.L. Dunlop, J. Appl. Phys. **66**, 3666 (1989)
4. G.Y. Sung, C.H. Kim, M.H. Oh, Adv. Ceram. Mater. **2**, 841 (1987)
5. D. Kovar, M.J. Readey, J. Am. Ceram. Soc. **79**, 305 (1996)
6. T. Takemura, M. Kobayashi, Y. Takada, K. Sato, J. Am. Ceram. Soc. **69**, 430 (1986)
7. J. Kim, T. Kimura, T. Yamaguchi, J. Mater. Sci. **24**, 2581 (1989)
8. D.R. Clarke, J. Appl. Phys. **50**, 6829 (1979)
9. JCPD 52-0114, International Center for Diffraction Data, JCPDs, Penn, USA (1983)
10. A. Rečnik, N. Daneu, T. Waltther, W. Made, J. Am. Ceram. Soc. **84**, 2657 (2001)
11. W. Jo, S.J. Kim, D.Y. Kim, Acta Mater. **53**, 4185 (2005)
12. E.M. Levin, C.R. Robbins, H.F. McMurdie, in *Phase diagrams for ceramists*, ed. By M.K. Reser (American Ceramic Society, Columbus, OH, 1964)
13. H. Wang, Y.M. Chiang, J. Am. Ceram. Soc. **81**, 89 (1998)
14. M. Inada, J. Appl. Phys. **19**, 409 (1980)
15. J.H. Choi, N.M. Hwang, D.Y. Kim, J. Am. Ceram. Soc. **84**, 1398 (2001)
16. J. Kim, T. Kimura, T. Yamaguchi, J. Mater. Sci. **24**, 2581 (1989)
17. M. Peiteado, J.F. Fernández, A.C. Caballero, J. Eur. Ceram. Soc. **25**, 2999 (2005)
18. C.H. Lu, N. Chyi, H.W. Wong, W.J. Hwang, Mater. Chem. Phys. **62**, 164 (2000)
19. J. Wong, J. Appl. Phys. **46**, 1653 (1975)
20. H.-T. Sun, L.-Y. Zhang, X. Yao, J. Am. Ceram. Soc. **76**, 1150 (1993)